Acceptor-bound magnetic polaron in $Cd_{1-x}Mn_xTe$ semimagnetic semiconductors

Tran Hong Nhung,* R. Planel, and C. Benoit à la Guillaume
Groupe de Physique des Solides de l'Ecole Normale Supérieure, Université Paris VII, 2 Place Jussieu, F-75251 Paris Cedex 05, France

A. K. Bhattacharjee
Laboratoire de Physique des Solides, Université de Paris—Sud, Bâtiment 510, F-91405 Orsay, France
(Received 13 February 1984)

Experimental data of donor-acceptor—pair time-resolved spectroscopy in $Cd_{1-x}Mn_xTe$ alloys are used to extract the acceptor binding energy as a function of temperature and composition. This is done between 1.6 and 35 K, and for compositions $x \leq 0.1$. The magnetic part of this energy is explained in terms of bound-magnetic-polaron formation. We present a statistical-mechanical theory that goes beyond the Gaussian approximation. It also takes into account the discrete spatial distribution of Mn^{2+} and the fact that the effective spin of the hole is $\frac{3}{2}$. Excellent agreement is obtained for the case of $x=0.05$.

I. INTRODUCTION

In recent years, numerous studies in semimagnetic semiconductors[1] (SMSC) have been devoted to bound magnetic polarons (BMP's); that is, the local ordering of magnetic moments in the orbit of a neutral impurity. This effect is due to exchange interaction between the d electrons of the dilute magnetic ions and the unpaired electron (or hole) bound to the shallow impurity.

These alloys exhibit, at least for small magnetic ion concentrations, semiconductor properties rather close to the ones of well-known binary compounds such as CdTe. As a consequence, optics provides an accurate method by which to understand magnetic properties, and, in particular, impurity spectroscopy can be used to study magnetization within the spatial extension of impurity states.

There is now comprehensive knowledge of donor-bound magnetic polarons (D^0-$\mathscr{P}$), which have been studied in n-type compounds $Cd_{1-x}Mn_xSe$ (Ref. 2) and $Cd_{1-x}Mn_xS$ (Refs. 3 and 4). The energy distribution of D^0-$\mathscr{P}$, which includes the effect of magnetic fluctuations,[5] can be precisely observed and calculated with remarkable agreement.[6,7]

The case of acceptor-bound magnetic polarons (A^0-$\mathscr{P}$) is more complex, from both experimental and theoretical points of view.

First, from the effective-mass ratio for conduction and valence bands in II-VI compounds, we expect the volume of interest around the acceptor center to be, roughly speaking, 100 times smaller than that for donors. It should result in a very large enhancement of the BMP effect. However, fluctuation effects should also be much more important, i.e., magnetic fluctuations and chemical broadening, through the number *and* position of Mn^{2+} ions in the hole orbit.

The first experimental observation of A^0-$\mathscr{P}$ in SMSC was the temperature-dependent binding energy of excitons bound to neutral acceptors.[8,9] However, it is difficult to obtain quantitative A^0-$\mathscr{P}$ results from these data: Both initial and final states of the observed transition A^0X are perturbed by the BMP effect.

Transport measurements made by Jaroszynski *et al.*[10] also provided evidence of an exchange contribution to the acceptor binding energy in $Cd_{1-x}Mn_xTe$. However, they were restricted to rather high temperatures ($T \sim 77$ K), so that the BMP effect is not clearly distinguished from the contribution of magnetic fluctuations. We did not observe spin-flip Raman scattering on A^0-$\mathscr{P}$, a technique which was used to directly investigate D^0-$\mathscr{P}$.

In order to study A^0-$\mathscr{P}$ on a quantitative basis, we measured the average binding energy of the complex as a function of temperature. This was done using time-resolved spectroscopy of donor-acceptor (D^0-A^0) luminescence.[11] In Sec. II we present these experiments and their analysis in detail greater than in Ref. 11. In Sec. III we present a relatively accurate statistical-mechanical calculation of the A^0-$\mathscr{P}$ energy. It involves a finite number of Mn^{2+} ions with a realistic arrangement on the fcc lattice and includes magnetic saturation and fluctuation effects. Comparison is made with our most reliable experimental results, obtained in $x=0.05$ compounds, and provides an excellent agreement with the data.

II. EXPERIMENT

A. Setup

Our experimental setup consisted of an argon laser connected to an acousto-optic modulator in order to obtain square pulses adjustable in intensity and length.

The sample was immersed either in the gas flow of an variable-temperature cryostat or in pumped liquid helium, in order to reach temperatures lower than 4.2 K. The photoluminescence was analyzed by an 8-Å/mm grating monochromator and detected by a cooled GaAs-cathode photomultiplier (PM).

Since such PM's have a rather low amplification factor, the signal was applied at the input of a low-noise rapid preamplifier, working in the ac coupling mode. It was then processed by a double-gate boxcar integrator, one gate being positioned before the exciting pulse and the other selecting delayed luminescence. Thus the difference between the two sampled signals was insensitive to the base line, that is, to the time-integrated signal. This procedure minimizes the distortion of the time-delayed spectra by delayed electronic influence of the integrated spectrum. It allowed us to use a high repetition rate, typically 50—100 kHz, and to discriminate, from the in-pulse luminescence, delayed luminescence that is smaller by 3 orders of magnitude, with 100-ns gatewidths.

Because the effects we were looking for were very sensitive to temperature, we had to give up the idea of saturating the donor-acceptor pairs by strong illumination, and preferred to attain some steady-state regime by using weak and long pulses. This was checked by observation of the luminescence spectrum during the exciting pulse. Appropriate conditions for this spectrum to reach a roughly constant shape before the end of the pulse were found to lie around 50 mW, focused, by a cylindrical lens, on 1 mm^2, during 1 μs. Thus, we obtained reproducible results and marked temperature effects, which is an *a posteriori* proof of good temperature control. Since the extraction from the data of the quantity of interest, the A^0 energy, is not straightforward and may be affected by systematic errors, great care was taken to maintain the same experimental conditions for all the investigated Mn compositions x and temperatures T. Reflectivity measurements were done to obtain accurately the free-exciton energy under the same (x,T) conditions. The samples we studied were grown at the Polish Academy of Science of Warsaw (Poland) or at Centre National de la Recherche Scientifique—Bellevue (CNRS—Bellevue) (France). Most of them were not intentionally doped, and samples from both origins provided comparable results. The few doped samples we used had been submitted to lithium diffusion.

B. Results

Most of the time-resolved luminescence spectra we observed are similar to the ones shown in Fig. 1. They were found in our $x \leq 0.05$ purest samples. As they turned out to be the most informative, we shall first discuss this type of spectra.

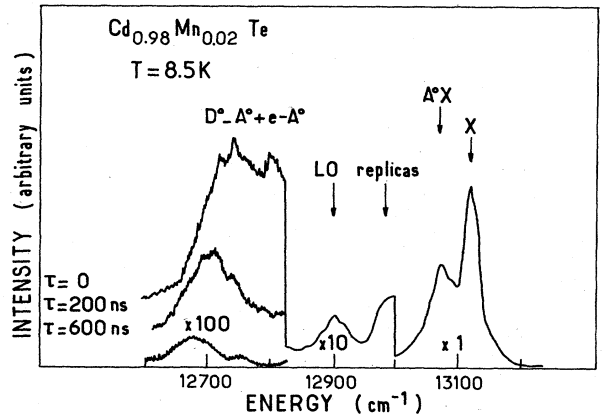

FIG. 1. Time-resolved luminescence spectra with different delays τ in a pure $Cd_{0.98}Mn_{0.02}Te$ sample.

1. *Luminescence spectrum in "pure" $x \leq 0.05$ samples*

Apart from line broadening and an energy-gap shift with composition,[12] the spectrum in Fig. 1 is quite comparable to the ones of rather pure CdTe samples at the same temperature. Two intense high-energy lines are attributed[13] to free (X) and acceptor-bound (A^0X) excitons, respectively, alloy broadening being more important on the latter due to the smaller spatial extension of the wave functions.

At lower energies, the LO-phonon replicas of these lines are identified as follows: They correspond to the CdTe-like LO mode observed in these alloys around 170 cm^{-1},[14] and the X-LO replica exhibits the asymmetric line shape observed in pure direct-gap semiconductors such as CdTe.

On the low-energy side of these excitonic lines, broader bands exhibit the characteristic features of donor-acceptor (D^0-A^0) recombination: Luminescence is observed after long delays compared to the typical excitonic recombination times, and the band shifts towards lower energies as the delay is increased. The energy $E_M(\tau)$ of the band maximum as a function of delay is plotted in Fig. 2 for various temperatures T and for a representative $x=0.05$ sample. The integrated band intensity is also plotted versus the delay; it roughly follows a power law at low temperatures, and for $\tau < 10$ μs, $I_{rad}(\tau) \propto \tau^{-1}$. However, it was difficult to detect delayed luminescence after, typically, 10 μs.

Around temperatures $T \sim 20$—30 K, the behavior of this band clearly changes: delayed luminescence disappears, which should be related to the ionization of donors. Thus, at high temperature, conduction-band—to—acceptor (e-A^0) recombination should dominate. To be exhaustive,

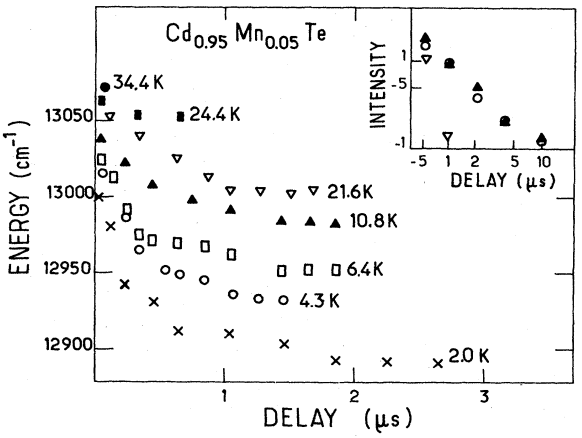

FIG. 2. Energy $E_M(\tau)$ of the maximum of the D^0-A^0 band in a pure $Cd_{0.95}Mn_{0.05}Te$ sample, as a function of delay τ, and at different temperatures. Note that in the range 20—25 K the behavior seems to be more characteristic of the e-A^0 transition. Inset shows the total intensity decay as $\log_{10}I$ vs $\log_{10}\tau$ for three selected temperatures. Note that the decay is faster than τ^{-1} around 20 K.

we also mention that the D^0-A^0 band we have studied is followed, on its low-energy side, by its LO-phonon replicas. At lower energies, some samples exhibit very broad and rather intense bands, which may be associated with the 1.42-eV band in CdTe. This band is often attributed to recombination on deep acceptors.[15]

To conclude the presentation of these luminescence results, we point out that the relative intensity of impurity bands in our undoped samples remains small compared to excitonic luminescence. It confirms the reasonable purity of these samples.

2. *Discussion of low-temperature results*

Now our aim is to extract from these data the *mean* energy of shallow acceptors for various compositions x and temperatures T. Actually, we expect the A^0 energy distribution to be broadened by composition and magnetic fluctuations.

The D^0-A^0 recombination is an old problem in semiconductor studies, but additional hypotheses are generally necessary to obtain a useful solution. Let us recall that the radiative energy of a given D^0-A^0 pair with a sufficiently large separation R is given by

$$E_{DA}(R)=E_G-E_A-E_D+e^2/\epsilon R \ , \tag{1}$$

where E_G, E_A, and E_D are, respectively, the energy gap, the A^0 and D^0 binding energy, and ϵ, the dielectric constant. On the other hand, the probability of radiative recombination $W(R)$ is proportional to the overlap of the wave functions. In the case where $a_D \gg a_A$,

$$W(R)=W_0\exp(-2R/a_D) \ . \tag{2}$$

We now must deal with the kinetics of D^0-A^0 pairs. Keeping in mind that we are concerned with undoped p-type materials, we first assume that compensation is small ($N_D \ll N_A$) and that impurity distribution is random. In this framework, the description of D^0-A^0 kinetics reduces to a statistical problem on donors considered isolated from one another. This problem was treated by Thomas *et al.*[16] and later by Döhler.[17] In the following discussion we treat the case of $x=0.05$ samples as an example. We shall first specify the key parameters of the problem and then consider this time-dependent situation step by step in order to test the internal consistency of the model.

We use typical CdTe values[18] for the donor binding energy $E_D=120\ \mathrm{cm}^{-1}$, the donor Bohr radius $a_D=50$ Å, and the dielectric constant $\epsilon=9.7$. We neglect the possible formation of a BMP around neutral donors during their lifetime; from the ratio of donor Bohr radii in CdSe and CdTe, and from D^0-$\mathscr{P}$ studies in n-type $Cd_{1-x}Mn_xSe$,[6,7] one easily deduces that this effect could increase E_D by $\sim 3\ \mathrm{cm}^{-1}$ at $T\sim 2$ K and would be negligible above $T\sim 5$ K.

The energy gap E_G is determined through

$$E_G=E_x(x,T)+\mathscr{R}_y \ , \tag{3}$$

where E_x is the free-exciton energy of the material, measured by a reflectivity experiment for given composition x and temperature T, and $\mathscr{R}_y$ is the free-exciton effective Rydberg energy, which is assumed to be constant and equal to the CdTe value: $\mathscr{R}_y=100\ \mathrm{cm}^{-1}$.

Other parameters are more difficult to estimate; we shall show during the following discussion that our results imply (i) that the quantity W_0 appearing in Eq. (2) should lie in the range $10^{10}<W_0<10^{11}\ \mathrm{s}^{-1}$, and (ii) that the acceptor concentration should satisfy $N_A<10^{16}\ \mathrm{cm}^{-3}$ in our "pure" samples (such values are consistent with transport measurements made on samples from the same origin[10]).

To describe the evolution of D^0 population, the relevant quantity is $Q(R,\tau)$, the probability of finding an electron on a donor as functions of its distance R from the nearest acceptor and of delay τ (after excitation has been switched off). At $\tau=0$ we have a steady-state regime where donors with small R values are essentially ionized. More precisely,[17]

$$Q(R,0)\sim\begin{cases}0 & \text{for } R<\bar{r}(I_{\mathrm{ex}}),\\ 1 & \text{for } R>\bar{r}(I_{\mathrm{ex}}),\end{cases}$$

where the quantity $\bar{r}(I_{\mathrm{ex}})$ depends on excitation during the steady-state regime through

$$\frac{I_{\mathrm{ex}}}{W_0N_D}\exp[2\bar{r}(I_{\mathrm{ex}})/a_D] = 1-\exp\{-(a_D/2\rho_A)^3[2\bar{r}(I_{\mathrm{ex}})/a_D]^3\} \ , \tag{4}$$

where a_D is the D^0 Bohr radius, ρ_A is the mean distance between acceptors,

$$\rho_A=(4\pi N_A/3)^{-1/3} \ , \tag{5}$$

and I_{ex} is the density of donors which are neutralized per second by the exciting light. To estimate I_{ex}, we assume that exciting light is absorbed within 0.1 μm. Thus, total excitation during the pulse is about 10^{24} photons $\mathrm{cm}^{-3}\,\mathrm{s}^{-1}$. Assuming, in addition, from the relative intensity of excitonic and D^0-A^0 luminescence, that at least 1% of excitation results in the neutralization of donors, we obtain $I_{\mathrm{ex}}>10^{22}$ photons $\mathrm{cm}^{-3}\,\mathrm{s}^{-1}$. Now using Eq. (4), with $W_0\leq 10^{11}\ \mathrm{s}^{-1}$, $n_D \leq n_A<10^{16}\ \mathrm{cm}^{-3}$, and $a_D=50$ Å, we obtain $r(I_{\mathrm{ex}})<250$ Å.

The temporal evolution of the donor population may then be described as follows:[17] For delay τ satisfying $W_0\tau\gg 1$ (which is, in practice, the case), neutral donors have essentially recombined if $R<\bar{r}(\tau)$, where $\bar{r}(\tau)$ depends on delay via

$$\bar{r}(\tau)=(a_D/2)\ln(W_0\tau/\ln 2) \ . \tag{6}$$

As a consequence, in a first stage, the D^0 population is not very dependent on delay:

$$Q(R,\tau)\sim Q(R,0) \quad \text{for } \bar{r}(\tau)<\bar{r}(I_{\mathrm{ex}}) \ .$$

In a second stage, for $\rho_A>\bar{r}(\tau)>\bar{r}(I_{\mathrm{ex}})$, the evolution is similar to the one following a strong flash excitation, such as that studied by Thomas *et al.*;[16] thus it is only slightly dependent on exciting conditions I_{ex} and acceptor concentration N_A. In this regime the total intensity follows a τ^{-1} decay law and the maximum $E_M(\tau)$ of the D^0-A^0 luminescence is shifted towards low energies through

$$E_M(\tau)=E_G-E_A-E_D+E_C(\tau)\ , \tag{7}$$

where $E_C(\tau)$, the mean Coulombic energy, is given by

$$W_0\tau=[1-E_C(\tau)/E_D]\exp[4E_D/E_C(\tau)]\ . \tag{8}$$

Lastly, in a third stage, $\bar{r}(\tau)$ becomes larger than ρ_A, and the luminescence decay is faster.

From our experimental results as summarized in Fig. 2, our regime of interest is clearly the second-stage regime, in the delay range $0.5<\tau<10\ \mu$s, and for temperatures lower than 10 K: The experimental curves $E_M(\tau)$ are almost parallel and exhibit a low-energy shift of (75 ± 5) cm^{-1} for $\tau=1\ \mu$s. Using Eq. (8) we deduce that $W_0\sim10^{10}$–$10^{11}\ s^{-1}$; then noting that $\bar{r}(\tau=10\ \mu s)>\rho_A$, we obtain, from Eqs. (5) and (6), that $\rho_A\geq350$ Å and $N_A\leq10^{16}\ cm^{-3}$. This is the point where we test the consistency of our analysis since W_0 and N_A are the parameters we had to estimate at the beginning.

We may also check, from Eqs. (4) and (6), that

$$\bar{r}(\tau=1\ \mu s)>250\ \text{Å}>\bar{r}(I_{ex})\ ,$$

as required in the second-stage regime.

To summarize, the model we used is self-consistent, at least for $T<10$ K, and we may deduce the acceptor energy $E_A(x,T)$ from the experimental $E_M(\tau)$ for a given (x,T) condition. From the above discussion, the conditions of lying in the second-stage regime are quite likely to be fulfilled around a delay of $\tau=1\ \mu$s. As a consequence, we can determine $E_A(x,T)$, using Eqs. (7) and (3), through

$$E_A(x,T)=E_x(x,T)+\mathscr{R}_y-E_M(\tau=1\ \mu s)+E_c(\tau=1\ \mu s)E_D\ , \tag{9}$$

where $E_C(\tau=1\ \mu s)=(45\pm5)\ cm^{-1}$ is deduced from Eq. (8). We estimate this uncertainty from the approximate fitting procedure we used. Moreover, a comparable uncertainty should be assumed for $E_M(\tau=1\ \mu s)$ due to experimental linewidths.

3. *Discussion of high-temperature results*

As the temperature is raised from, typically, 10 to 20 K, the total intensity decay is faster than that at low temperature (see Fig. 2): we expect the D^0 lifetime to be limited by thermal effects. However, since a pronounced low-energy shift is still observed on $E_M(\tau)$ curves, it is reasonable to suppose that thermal ionization of donors is not sufficiently important to destroy the consistency of our model, which is, within this limit, temperature independent. Thus we extract the acceptor binding energy from Eq. (9) up to $T\sim20$ K.

On the contrary, as the temperature increases from 20 to 25 K, a clearcut change is observed: Delayed luminescence almost disappears, which is quite consistent with the ionization of donors if their concentration lies around $N_D\sim10^{15}\ cm^{-3}$. As a consequence, luminescence in this high-temperature regime ($T>25$ K) is better described in terms of conduction-band–to–acceptor (e-A^0) transitions. Thus, we get acceptor energy through

$$E_A(x,T)=E_x(x,T)+\mathscr{R}_y-E_M(\tau=0)+k_BT/2\ , \tag{10}$$

where $E_x(x,T)+\mathscr{R}_y$ is the energy gap.[19]

The resulting $E_A(x,T)$ for all investigated temperatures and compositions are plotted in Fig. 3. It is important to note that these curves do not exhibit any discontinuity around $T\sim25$ K, although the fitting procedures are quite different below and above this temperature. Moreover, the fitting procedure we used provides a constant acceptor energy $E_A(0,T)$ in the case of pure CdTe, as expected. These are two *a posteriori* tests for its validity.

4. *"Impure" samples*

Some of our investigated samples exhibited a somewhat different behavior. Although the luminescence spectrum was roughly comparable to the previous case, delayed luminescence of the D^0-A^0 band decayed more rapidly and the associated energy shift was much less pronounced. We think this behavior, which is observed without systematic dependence on composition, is due to a higher impurity concentration. Actually, within the framework of the model we used, it is easily shown that if $N_A\sim10^{17}\ cm^{-3}$, ρ_A is reduced to, typically, 100 Å; as a result, the most probable D^0-A^0 Coulomb energy is of the order of 120 cm^{-1}, and luminescence decays rapidly after 10^{-8} s. Another possible interpretation could be a drastic reduction of D^0 nonradiative lifetime, which is not included in the model. In both cases, most probable pair energies are resonant with the e-A^0 transition. Therefore, a detailed study of D^0-A^0 statistics would be hazardous and we think it more reasonable to extract A^0 energies from the $\tau=0$ spectra, using Eq. (10), as in the case of clear e-A^0 transitions. Within larger experimental uncertainties, this procedure provides results consistent with those of purer samples.

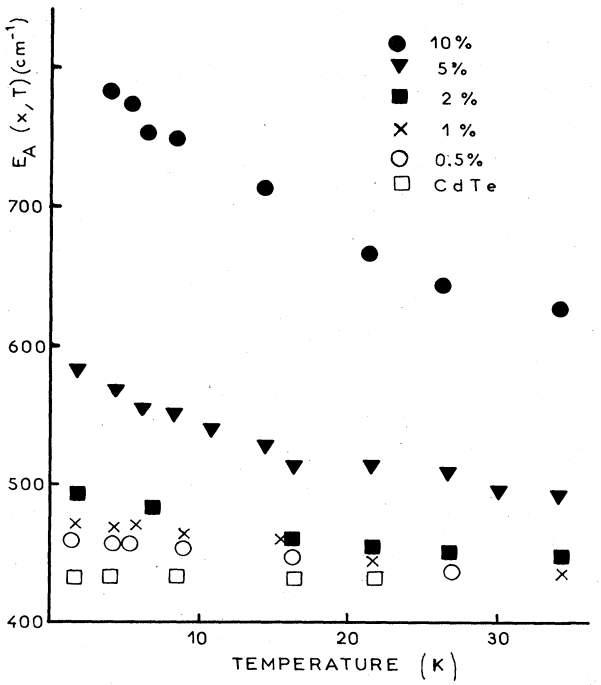

FIG. 3. Experimental mean acceptor energy $E_A(x,T)$ as a function of temperature T and for various compositions x.

5. $x \geq 0.10$ samples

In $x=0.10$ samples the situation is always found to be qualitatively different. Over the entire temperature range of interest, the luminescence spectra are dominated by a broad asymmetric line (see Fig. 4) which has been attributed to excitons localized on composition and/or magnetic fluctuations.[9] In undoped samples there is no structure in the steady-state spectra to be attributed to impurity recombination. However, delayed spectroscopy improves the contrast and favors the observation of weak bands which may be associated with D^0-A^0 transitions.

To improve our results an attempt was made on lithium-diffused samples: lithium is known to act, in CdTe, either as an acceptor or as a donor, depending on its location in the crystal lattice. Actually, these doped samples exhibited broad luminescence bands at the same energy as delayed luminescence in pure samples, but the impurity density was too high to study precisely the D^0-A^0 kinetics, as in the case of impure samples described in Sec. II B 4. In brief, Li doping helped identify D^0-A^0 recombination, but did not improve the accuracy of our measurements. Therefore, to determine A^0 energies for $x=0.10$, we essentially used undoped samples, employing the same fitting procedure described in Sec. II B 2. However, due to the roughness of these results (weak and broad bands), the validity of the model remains uncertain. For example, we have no clearcut indications that compensation is negligible and that a reasonable fraction of donors is *neutralized* during excitation. In fact, we think that the localization of excitons may explain the relative decrease of impurity luminescence for reasonable impurity concentrations. An attempt to extend our study to higher-Mn-concentration samples ($x=0.20$) led to similar conclusions. Our experimental approach, in which we apply rather sophisticated methods of semiconductor spectroscopy to these alloys, should be restricted to the low-x range ($x<0.10$) to remain on a firm basis.

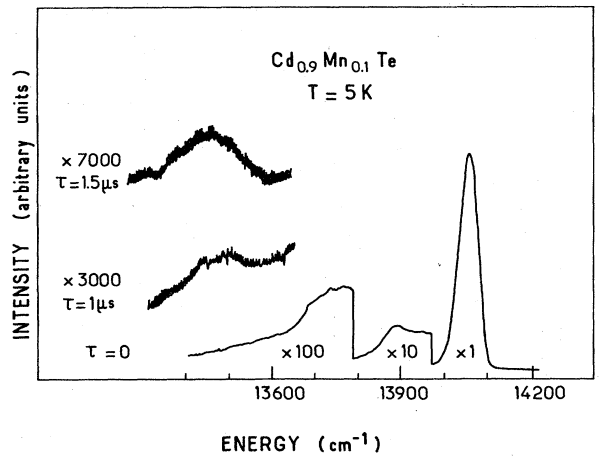

FIG. 4. Time-resolved luminescence spectra in an undoped $Cd_{0.90}Mn_{0.10}Te$ sample. Note the small relative intensity of delayed luminescence.

III. THEORY

A bound magnetic polaron consists of an electron (hole) bound to a donor (acceptor) impurity, and interacts with magnetic ions (Mn^{2+}) within its orbit through the exchange interaction. This interaction gives rise to a mutual spin polarization of the electron (hole) and the Mn^{2+} ions, thus yielding an additional binding energy. This magnetic contribution to the binding energy decreases with increasing temperature. Here we present a statistical-mechanical model for the BMP energy, starting from the Heisenberg-type exchange Hamiltonian used by Golnik *et al.*[8]

Recent theoretical models (macroscopic[5] and microscopic[6]) go beyond the simple "molecular-field" approximation of Ref. 8 by taking into account Gaussian fluctuations of the effective field due to Mn spins acting on the bound-electron (-hole) spin. The Gaussian approximation appears to be adequate for describing the D^0-$\mathscr{P}$ in $Cd_{1-x}Mn_xSe$,[6,7] where the mean number N of Mn ions in the impurity orbit is sufficiently large (~ 100) and the coupling is weak. On the contrary, in the case of A^0-$\mathscr{P}$ in $Cd_{1-x}Mn_xTe$, $N\sim 10$, and it is necessary to go beyond the Gaussian approximation. In Ref. 11 a phenomenological model was given for calculating the acceptor energy as a function of temperature. However, this model takes into account the saturation of Mn^{2+} spins in a very crude way. It predicts a rather steep, although not diverging, energy, as $T\to 0$. In the following, we present a statistical-mechanical model that is in excellent agreement with experimental data.

We consider a realistic arrangement of Mn^{2+} ions on the fcc lattice around the impurity center (assumed to be situated at a Cd site). This is done over successive shells of the lattice up to a cutoff distance. Thus we can calculate the partition function in a straightforward manner by assuming that the Mn^{2+} spins are classical vectors. This allows us to calculate the average binding energy as a function of temperature, without further approximations regarding the exchange field.

We start from the Heisenberg-type Hamiltonian:

$$\mathscr{H}=-J\vec{s}\cdot\sum_i b_i\vec{S}_i\ , \tag{11}$$

where

$$b_i=|\phi(\vec{R}_i)|^2\ . \tag{12}$$

$\phi(\vec{R})$, being the impurity envelope function, is assumed to be hydrogenic:

$$\phi(\vec{R})=(\pi a_B^3)^{-1/2}e^{-R/a_B}\ . \tag{13}$$

Here, a_B is the Bohr radius, $\vec{R}_i$ is the position vector of the ith Mn ion, and $\vec{S}_i$ is its spin operator ($S=\frac{5}{2}$). $\vec{s}$ is the spin of the electron ($s=\frac{1}{2}$) or the effective spin of the hole ($s=\frac{3}{2}$). J is the exchange parameter. Usually,[1,20] this is quoted in terms of $N_0\alpha=N_0J$ for an electron and $N_0\beta=3N_0J$ for a hole, where N_0 is the number of cation sites per unit volume.

In order to deal with this Hamiltonian without making the continuum approximation for the distribution of Mn, we cut off the infinite sum by setting

$$b_i=0 \text{ for } R_i>R_c \ . \tag{14}$$

This allows us to treat a finite number N of Mn^{2+} ions. Physically, R_c is the distance where the effective hole-Mn exchange interaction becomes comparable in size to the small Mn-Mn antiferromagnetic interaction which is neglected. We shall treat R_c as an empirical parameter.

We now treat the Mn spins as classical vectors:

$$\vec{S}_i=S\hat{n}_i \ , \tag{15}$$

where $\hat{n}_i$ is a unit vector. The partition function is then given by

$$Z=\sum_{m=-s}^{s}\int d\Omega_1\int d\Omega_2\cdots\int d\Omega_N \exp\left[\bar{\beta}J\vec{s}\cdot\sum_{i=1}^{N}b_i\vec{S}_i\right] \tag{16}$$

(with $\bar{\beta}=1/k_BT$), where the sum is over the magnetic quantum number m of the electron (hole) spin, and the range of integration over $d\Omega_i$ is the full solid angle, $d\Omega_i$ being the solid-angle element around $\hat{n}_i$. Equation (16) can be rewritten as

$$Z=(4\pi)^N\sum_{m=-s}^{s}\int d\vec{M}\,P(\vec{M})e^{\bar{\beta}J\vec{s}\cdot\vec{M}} \ , \tag{17}$$

where

$$P(\vec{M})\equiv\frac{1}{(4\pi)^N}\int d\Omega_1\int d\Omega_2\cdots\int d\Omega_N\,\delta\left[\vec{M}-\sum_i b_i\vec{S}_i\right] \tag{18}$$

is the probability that the sum of the N spin vectors, weighted by the b_i factor, is $\vec{M}$ when all orientations are equally probable for each one of them. This represents the probability distribution of the effective field acting on $\vec{s}$.

By calculating the sum in Eq. (17), we obtain

$$Z=(4\pi)^N\int d\vec{M}\,P(\vec{M})z(\vec{M}) \ , \tag{19}$$

with

$$z(\vec{M})=\sinh\left[(2s+1)\frac{\bar{\beta}JM}{2}\right]\Big/\sinh\left[\frac{\bar{\beta}JM}{2}\right] . \tag{20}$$

Thus we may extract all the thermodynamic quantities of interest. In our case, the mean energy is then given by

$$\bar{E}=-\int d\vec{M}\,P(\vec{M})\frac{\partial}{\partial\bar{\beta}}z(\vec{M})\Big/\int d\vec{M}\,P(\vec{M})z(\vec{M}) \ . \tag{21}$$

We can see directly from Eq. (18) that $P(\vec{M})$ vanishes for M above

$$M_{\max}=S\sum_{i=1}^{N}b_i \ . \tag{22}$$

This fixes the upper limit of the integrals in Eq. (21). It is interesting to study the limiting behavior of energy as a function of temperature directly from Eq. (21). We obtain

$$\bar{E}=-|J|sM_{\max} \text{ as } T\to 0 \ , \tag{23}$$

which is, in fact, the quantum-mechanical ground-state energy. On the other hand,

$$\bar{E}=-\tfrac{4}{3}s(s+1)\bar{\beta}(J/2)^2\sum_{i=1}^{N}b_i^2S^2 \text{ as } T\to\infty \ , \tag{24}$$

which is the well-known $1/T$ behavior at high temperature. It should be noted that a quantum-mechanical calculation (high-T expansion of the density matrix) yields $S(S+1)$ instead of S^2 in Eq. (24).

Clearly, for calculating $\bar{E}$ for an arbitrary T, we must evaluate $P(M)$. If N is so large that $\sqrt{N}\gg 1$, we can apply the central-limit theorem[21] in Eq. (18) and obtain the Gaussian distribution:

$$P_G(\vec{M})=(2\pi A)^{-3/2}e^{-M^2/2A} \ , \tag{25}$$

where

$$A=\tfrac{1}{3}S^2\sum_i b_i^2 \ . \tag{26}$$

We recall that this approximation gives good results in the D^0-$\mathscr{P}$ case.[6] A straightforward application of this effective-field distribution yields

$$\bar{E}=-\frac{J^2A}{4}\bar{\beta}\left[1+\frac{2}{1+(J^2A/4)\bar{\beta}^2}\right] . \tag{27}$$

This describes the high-temperature behavior correctly, but diverges as $T\to 0$. The divergence problem, however, does not arise if we properly cut off the Gaussian at $M_{\max}$.

However, in the A^0-$\mathscr{P}$ in $Cd_{1-x}Mn_xTe$, N is relatively small (~ 10) and we must calculate $P(M)$ more precisely. For this purpose we use the Fourier integral representation of the δ function in Eq. (18) and obtain

$$P(\vec{M})=\frac{1}{(2\pi)^3}\int d\vec{k}\,e^{i\vec{k}\cdot\vec{M}}\prod_{j=1}^{N}\frac{1}{4\pi}\int d\Omega_j e^{-ib_j\vec{S}_j\cdot\vec{k}} \ . \tag{28}$$

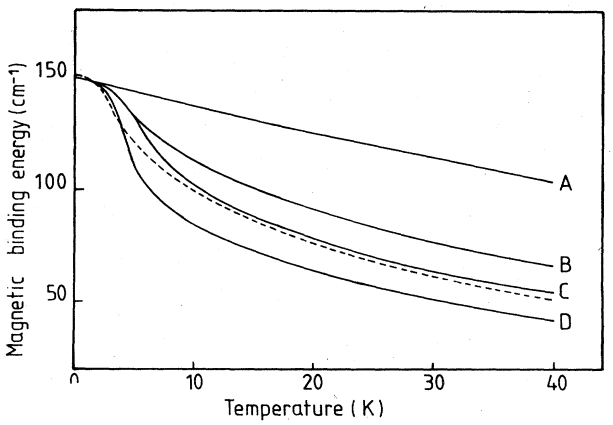

FIG. 5. Theoretical curves for the exchange contribution for the acceptor binding energy as a function of temperature. The solid curves A, B, C, and D correspond to the same Bohr radius $a_B=10$ Å, but different values for the cutoff radius: $R_c=10$, 13, 15, and 17 Å, respectively. The exchange parameter and the Mn arrangement are given in the text. The dashed curve corresponds to $a_B=12$ and $R_c=15$ Å.

We can carry out the angular integrals. Thus,

$$P(\vec{M})=\frac{1}{2\pi^2}\int_0^\infty dk\,k^2\frac{\sin kM}{kM}\prod_{i=1}^{N}\frac{\sin kSb_i}{kSb_i}\ . \tag{29}$$

For $N\leq 3$ this integral can be found in standard tables.

For $N>3$ we compute the integral numerically, with particular regard to convergence, especially for the small values of P when M approaches $M_{\max}$. The low-temperature behavior of the binding energy is very sensitive to this region.

For $s=\frac{3}{2}$ (hole) the energy can then be computed from

$$\bar{E}=-\left[\frac{3J}{2}\right]\frac{\left[\int_0^{M_{\max}}M^3P(\vec{M})\left[\sinh\frac{3\bar{\beta}JM}{2}+\frac{1}{3}\sinh\frac{\bar{\beta}JM}{2}\right]dM\right]}{\left[\int_0^{M_{\max}}M^2P(\vec{M})\left[\cosh\frac{3\bar{\beta}JM}{2}+\cosh\frac{\bar{\beta}JM}{2}\right]dM\right]}\ . \tag{30}$$

We present some results of this theory in Fig. 5. We assume that the impurity center is located at a Cd site. The successive neighboring shells of the fcc lattice are then enumerated in terms of the distance from the center and the number of sites. (See, for example, the table on p. 1037 of Ref. 22.) A mean arrangement for the Mn ions is then worked out, accounting for the proportion x of Mn in $Cd_{1-x}Mn_xTe$. The arrangement is specified in terms of the mean number n_j of Mn at the average distance r_j. We mention in passing that we have numerically verified that fluctuations of this arrangement hardly affect the mean value $\bar{E}$ that interests us. However, for calculating quantities such as line shape, a precise statistics of the distribution of Mn over the cation sublattice must be taken into account.

All the curves in Fig. 5 correspond to $x=0.05$. The solid curves *A*, *B*, *C*, and *D* correspond to the same Bohr radius $a_B=10$ Å, but different cutoff radii: $R_c=10$, 13, 15, and 17 Å, respectively. The exchange parameter is chosen so that the magnetic binding energy $|\bar{E}|=150\ \text{cm}^{-1}$ at 0 K. The Mn arrangements and the exchange values are listed below as follows:

For curve *A*, $N_0\beta=7708\ \text{cm}^{-1}$: $n_1=1, r_1=0.8a$; $n_2=1, r_2=1.225a$; $n_3=1, r_3=1.414a$.

For curve *B*, $N_0\beta=5024\ \text{cm}^{-1}$: $n_1=1, r_1=0.8a$; $n_2=1, r_2=1.225a$; $n_3=2, r_3=1.525a$; $n_4=3, r_4=1.871a$.

For curve *C*, $N_0\beta=4315\ \text{cm}^{-1}$: n_j, r_j ($j=1$–4) same as for curve *B*; $n_5=3, r_5=2.167a$.

For curve *D*, $N_0\beta=3644\ \text{cm}^{-1}$: n_j, r_j ($j=1$–5) same as for curve *C*; $n_6=6, r_6=2.489a$.

Here, $a=6.48$ Å is the lattice constant. The dashed curve in Fig. 5 corresponds to the same Mn arrangement and R_c as the solid curve *C*, but a different Bohr radius $a_B=12$ Å. The exchange parameter $N_0\beta=5500\ \text{cm}^{-1}$ is chosen to match curve *C* at $T=2$ K. Clearly, the cutoff radius R_c, which determines the number N of Mn ions enclosed in the BMP (for a given composition x), is a crucial parameter for the binding-energy—versus—temperature curve. On the other hand, a variation of a_B for a fixed R_c appears to be less significant. One should, however, keep in mind that R_c must vary with a_B and x if our physical interpretation of the cutoff radius is valid.

In Fig. 6, we compare a theoretical curve (*C* of Fig. 5) with the experimental points (of Fig. 3) for $Cd_{0.95}Mn_{0.05}Te$. The agreement is excellent. The dashed curve in Fig. 6 results from the truncated Gaussian approximation discussed after Eq. (27), the parameters being the same as for the solid curve. It is clear that the Gaussian approximation is inadequate for explaining the experimental data.

Let us now discuss the parameters of our "best-fit" curve:

(1) The value $a_B=10$ Å is estimated as follows. From the measured value of the acceptor binding energy E_A and dielectric constant in CdTe,[23] we have $a_B=13$ Å. If we allow for a first-order correction due to polaron formation, we find, from a variational calculation, that a_B should be reduced by about 25%.

(2) $N_0\beta=4315\ \text{cm}^{-1}$. The free-hole value[20] is 7000 cm^{-1}. According to the estimations of Mycielski and Rigaux,[24] for a bound hole, $N_0\beta\sim 5200\ \text{cm}^{-1}$.

(3) The cutoff radius $R_c=15$ Å. The hole-Mn interaction at this distance is 4.6 $\text{cm}^{-1}=6.6$ K. A mean Mn-Mn—interaction parameter of $6.6/5\sim 1.3$ K would be consistent with this value. In fact, the nearest-neighbor Mn-Mn antiferromagnetic interaction parameter is estimated to lie between 1 and 6 K.[1]

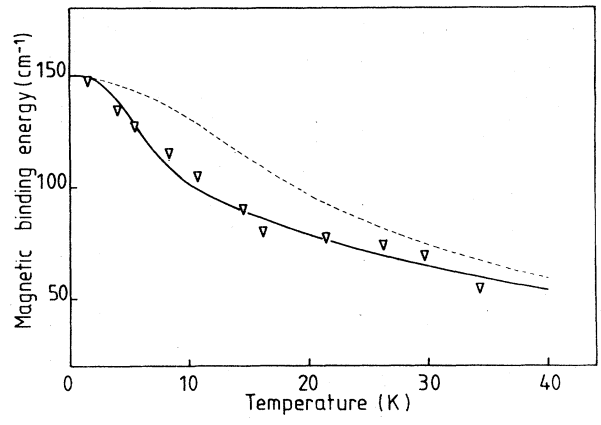

FIG. 6. Comparison between theory and experiment. The solid curve is curve *C* of Fig. 5 and the inverted triangles represent experimental points for $Cd_{0.95}Mn_{0.05}Te$. The dashed curve corresponds to a truncated Gaussian approximation.

We have more qualitative evidence in favor of the cutoff hypothesis. Although we have chosen to present theoretical results only for $x=0.05$, we have carried out some calculations for the $x=0.02$ case. We find it necessary to take a larger cutoff radius in order to account for the experimental data in this more dilute alloy.

IV. CONCLUSION

As explained in the Introduction, the acceptor-BMP is a more difficult problem from both theoretical and experimental points of view, as compared to the donor-BMP. The experimental method that we have employed, namely time-resolved spectroscopy of donor-acceptor pairs, for studying the acceptor-BMP, is certainly less accurate than the spin-flip Raman scattering method applicable to the donor-BMP. However, the error arising from the relatively indirect nature of the method is comparable to the unavoidable chemical and magnetic broadening. We have thus obtained unambiguous quantitative data for the binding energy as a function of temperature from 1.6 to 35 K for $x \leq 0.05$.

The theory we have presented describes both the low-temperature saturation and higher-temperature fluctuation regimes in a consistent manner. Our model differs from the ones applied until now in SMSC. Firstly, we do *not* make the Gaussian approximation. Secondly, the spatial distribution of the Mn ions over the cation sublattice is taken into account; this may also provide a basis for a more complete description of composition broadening. Thirdly, we take $s=\frac{3}{2}$ for the effective spin operator of the hole. Finally, we quantitatively account for the experiment without using the macroscopic parameters S_0 (reduced spin length) and T_0 (Curie-Weiss temperature). We introduce, instead, a cutoff radius R_c, which is related to the average value of the Mn-Mn exchange interaction.

ACKNOWLEDGMENTS

We are grateful to R. R. Gałazka of the Polish Academy of Sciences, Warsaw, Poland, and R. Triboulet of CNRS—Bellevue, France, who provided us with excellent samples.

*Permanent address: Institute of Physics, Hanoi, Vietnam.

[1]See the review paper by M. Grynberg, Physica (Utrecht) **117&118B**, 461 (1983), and references cited therein.

[2]M. Nawrocki, R. Planel, G. Fishman, and R. Gałazka, J. Phys. Soc. Jpn. Suppl. A **49**, 823 (1980); Phys. Rev. Lett. **46**, 735 (1981).

[3]D. Heiman, Y. Shapira, and S. Foner, Solid State Commun. **45**, 899 (1983).

[4]D. Alov, S. Guvarev, and V. Timofeef, Pis'ma Zh. Eksp. Teor. Fiz. **34**, 76 (1981) [JETP Lett. **34**, 71 (1981)].

[5]T. Dietl and J. Spałek, Phys. Rev. Lett. **48**, 355 (1982); Phys. Rev. B **28**, 1548 (1983).

[6]D. Heiman, P. A. Wolff, and J. Warnock, Phys. Rev. B **27**, 4848 (1983).

[7]R. Planel, Tran Hong Nhung, G. Fishman, and M. Nawrocki, J. Phys. (Paris) **45**, 1071 (1984).

[8]A. Golnik, J. A. Gaj, M. Nawrocki, R. Planel, and C. Benoit à la Guillaume, J. Phys. Soc. Jpn. Suppl. A **49**, 819 (1980).

[9]A. Golnik, J. Ginter, and J. A. Gaj, J. Phys. C **16**, 6073 (1983).

[10]J. Jaroszyński, T. Dietl, M. Sawicki, and E. Janik, Physica (Utrecht) **117&118B**, 473 (1983).

[11]Tran Hong Nhung and R. Planel, Physica (Utrecht) **117&118B**, 488 (1983).

[12]N. T. Khoi and J. A. Gaj, Phys. Status Solidi B **83**, K133 (1977).

[13]R. Planel, J. Gaj, and C. Benoit à la Guillaume, J. Phys. (Paris) Colloq. **41**, C5-39 (1980).

[14]W. Gebicki, A. Amzallag, M. Picquart, C. Julien, and M. Le Postollec, J. Phys. (Paris) Colloq. **41**, C5-339 (1980).

[15]T. Taguchi, J. Shirajuji, and Y. Inuishi, Jpn. J. Appl. Phys. **12**, 1558 (1973).

[16]D. G. Thomas, J. J. Hopfield, and W. M. Augustyniak, Phys. Rev. **140**, A202 (1965).

[17]G. H. Döhler, Phys. Status Solidi B **45**, 705 (1971).

[18]J. R. Panossian, A. A. Gippius, and V. S. Vavilov, Phys. Status Solidi **35**, 1069 (1969).

[19]A typographical error is to be corrected in the corresponding equation of Ref. 11.

[20]J. A. Gaj, R. Planel, and G. Fishman, Solid State Commun. **29**, 435 (1979).

[21]See, for example, C. Kittel, *Elementary Statistical Physics* (Wiley, New York, 1958), p. 129.

[22]J. O. Hirschfelder, C. F. Curtiss, and R. B. Bird, *Molecular Theory of Gases and Liquids* (Wiley, New York, 1954).

[23]L. Svob, Y. Marfaing, M. Hoclet, P. Plumelle, and M. Vandevyder, Solid State Commun. **28**, 895 (1978).

[24]J. Mycielski and C. Rigaux, J. Phys. (Paris) **44**, 1041 (1983).